N74-10267

Paper No. 41

PROPERTIES OF A CLOSED PORE INSULATION THERMAL PROTECTION SYSTEM*

A. Tobin, C. Feldman, M. Russak, and J. Reichman,
Research Department, Grumman Aerospace Corporation, Bethpage, New York 11714

ABSTRACT

The need to develop a 100 mission reusable external thermal protection system for the Space Shuttle Orbiter has led to the development of a unique closed-cell glass ceramic foam insulation derived from sintering fly ash cenospheres in the presence of a high emittance binder. The outstanding characteristics of this material are: (1) rigidity, (2) water repellant structure, (3) high emittance, (4) machinability, (5) outstanding mechanical properties, and (6) good thermal shock resistance. Detailed design integration studies have led to the construction and testing of scaled-up heat shield panels which have survived re-entry cycling in Areas 1 and 2 of the Shuttle.

The need to develop a 100 mission reusable thermal protection system for the Space Shuttle Orbiter has led to the investigation of lightweight, refractory ceramic insulation materials. Recent activities have shown that promising low density silica fibrous insulations require complex brittle coatings to provide a water repellant, erosion resistant, high emitting surface because the substrate materials have low strength and readily absorb moisture.

To overcome these inherent problems associated with fibrous materials a unique closed-cell glass-ceramic foam insulation material (CPI = closed pore insulation) was developed from sintering low cost hollow alumino-silicate glass microspheres (obtained from fly ash residues) with high emittance binders. The outstanding characteristics of this material are: (1) rigidity, (2) water repellancy, (3) high emittance, (4) machinability, (5) superior mechanical properties when

*This work was partially sponsored by the NASA Langley Research Center under Contract No. NAS1-10713 and the Johnson Spacecraft Center under Contract No. NAS9-12781.

522-137 O - 73 - 37

compared to rigidized fibrous insulations, and (6) good thermal shock resistance.

The processing variables are closely related to the mechanism of the foam formation. An optimum firing rate was necessary to form the closed cell structure since the forces of expansion of the residual gas entrapped within each cenosphere are balanced by the forces of contraction due to the sintering, viscous flow of the glassy shell, and atmospheric pressure. Final cell sizes are related to the temperature, time, and cobalt oxide additive. Increasing temperature and cobalt level led to increasing pore size (Fig. 1) and decreased softening point of the glass.

X-ray data indicated the presence of mullite, cobalt aluminate, and a residual glass phase. Tables 1 and 2 lists the principal thermo-physical properties of CPI tiles.

TABLE 1 TYPICAL PHYSICAL PROPERTIES OF CPI - 4% CoO

Microstructure	Network of Closed Cells
Color	Brown-Blue
Density (Kg/m^3)	640-720
Wt % Water Absorption	0.5-4
Average Pore Size	80 μm
Available Sizes (cm)	20 x 20 x 2.5
Available Shapes	Flat Tile
Machinability	Machinable Ceramic Within 0.005 cm Tolerance

TABLE 2 CHEMICAL & THERMAL PROPERTIES OF CPI - 4% CoO

Chemistry	Al_2O_3, SiO_2, CoO, Fe_2O_3, TiO_2
Chemical Stability	Inert to Most Reagents
Thermal Expansion	$5.4 \times 10^{-6}/K$
Thermal Stability	No Disruptive Internal Changes on Cycling
Softening Point of CPI Glass	1310K
Emissivity (Uncoated)	0.63 - .65
Emissivity (Coated)	.82 - .88

Thermal expansion increased with cobalt additions due to the increasing concentration of cobalt aluminate in the glass. Total normal emissivity increased with cobalt additions over the range of temperatures investigated (RT-1500K). Emissivity

of CPI tiles was relatively independent of temperature. Increasing cobalt additions appeared to reduce the thermal conductivity of the foam at elevated temperatures. This may be due to the increased radiation absorption contribution of the cobalt ion in the glass. Theoretical calculations have shown that the radiation scattering and absorption component of the thermal conductivity are of the same magnitude (Ref. 1). This is in contrast to fibers where the scattering component dominates. In addition, solid conduction through the foam makes a substantial contribution to the total thermal conductivity.

Differential thermal analysis has shown no physical or chemical changes occurring over the range of temperatures investigated (RT-1700K).

To assess the possibility of employing these foams in a mechanical attachment scheme, a detailed characterization of the mechanical properties of CPI materials -- including elastic modulus tension, compression, flexure and shear at room and elevated temperatures -- was undertaken (Refs. 2 and 3). Figures 2 through 5 illustrate the general trends. Increasing cobalt oxide levels caused a reduction in the softening point of the glass, resulting in corresponding large decreases in elastic modulus and strength above 1135K with large increases in ductility. In fact, a large strain rate dependence of the strength was noted above 1175K. No significant degradation of strength properties was observed after 20 hrs of exposure in vacuum to 1380K. It should be noted that the strengths reported are one to two orders of magnitude higher than those reported for RSI materials. It was noted that CPI-4 had overall significantly superior mechanical properties than CPI-8 and CPI-12 for similar bulk densities (Fig. 6). This may be due to the finer and more uniform pore size of CPI-4 leading to a smaller probability of finding a critical flaw that will propagate to failure.

The significantly higher strength of CPI over conventional RSI materials is related to the continuous network of cell walls which can support a much larger load than a structure which is held together only at fiber intersections.

To assess the elevated temperature creep characteristics of CPI materials, a flexural creep apparatus was constructed which allowed measurements of the deflection of a flexural bar with varying continuous loads applied along its length. The deflections were recorded photographically while the specimens remained in the furnace. Creep deflections depended strongly on temperature, time and cobalt level; the lower cobalt level being the most creep resistant (Fig. 7). This is consistent with

the relationship between creep and glass viscosity ($\varepsilon \sim \eta \sim Ae^{-E/kT}$).

In order to assess the ability of CPI materials to resist simulated re-entry heating, a radiant heat lamp and a plasma arc jet (Refs. 2 and 4) were employed. The radiant heat lamps were programmed to simulate the Area 1, Area 2, and Area 2P shuttle heating profile (Fig. 8). CPI plates of varying thickness (backed by low density fibrous insulation to simulate the correct heat transfer conditions) were tested (Ref. 2). The following observations were made: (1) the maximum thickness above which thermal stress cracks were observed was 1.25 cm; (2) CPI plates have withstood 920K temperature drops across their thickness without thermal stress failure; (3) a slight buckling of CPI plates occurred at higher cobalt levels and at higher temperatures during thermal cycling; (4) the effect disappeared at below 1275K for CPI-12, 1360K for CPI-8, and 1530K for CPI-4; (5) 1.25 cm plates of CPI-4 withstood 25 cycles of Area 2P re-entry exposure with no observable changes; (6) no observable degradation of thermal or mechanical properties of CPI-8 and CPI-12 was found after 25 cycles of re-entry exposure; (7) plasma arc jet tests of CPI materials have shown a slight discoloration of the surface possible due to cobalt evaporation from the surface.

Simulated salt spray exposure tests were conducted on 2.54 cm diameter CPI-4 disc samples, which had a cobalt rich surface layer (Ref. 5). A fine sea water mist was sprayed on the samples and dried to leave a salt residue. A sprayed and a control (unsprayed) sample were then cycled in an electric furnace to simulated area 2P re-entry heating. The test sample was re-sprayed after each cycle. As cycling progressed, a glazing effect was noted on the surface of the test specimen. This was evidenced by a deformation of the surface pore structure and was attributed to the fluxing effect of the alkali element present in salt mist deposited on the sample. After 20 cycles, several hairline surface cracks was observed, which accounted for an increase in water absorbtion of the sample from approximately 2.7% to 6.8%. Electron microprobe analysis indicated an increase in alkali concentration in the crack vicinity. The effect of this increased alkali level was to locally increase the thermal expansion of the CPI, in turn lowering the material's thermal shock resistance, giving rise to fine surface microcracking. Microprobe studies across the interface region near the crack showed an increase in sodium concentration, thus accounting for a higher local expansion area in the crack vicinity.

Rain erosion tests on CPI tiles were conducted at AFML-Bell Aerospace Rain Erosion Test Facility (Ref. 6). Angles of attack varied from 10^{o} - 40^{o}. Rain velocities varied from $32\text{-}64 \times 10^{4}$ m/hr for periods of up to 1 hr. Erosion weight losses were dependent on angle of attack and rain velocity; however, loss of surface material did not result in the destruction of the tile or loss in water proofness due to the monolithic nature of CPI (Ref. 7).

As the thermal shock resistance and the higher density of CPI became a major design constraint, it became clear that a "composite" type heat shield would be required in which the CPI surface was backed by a lower density efficient fibrous high temperature insulation, which was appropriately packaged. Such a design then reduces thermal shock by reducing the temperature gradients through the CPI and consequently reduces weight. Two basic variations evolved from these concepts: (1) a mechanically fastened heat shield (Fig. 9) and (2) a bonded heat shield (Fig. 10).

In Fig. 9 a CPI tile is supported on 4 superalloy studs which are "bonded" into the tile using a CPI washer-retainer. The studs fit into a sliding bushing, whose motion accommodates the thermal and mechanical stresses acting on the tile during launch and re-entry. A bag of lightweight insulation fits under the CPI tiles which are pierced by the superalloy studs and is mechanically fastened to the primary structure. This design features a fail-safe capability along with increased ease of inspection, replacement and removal. In the second concept (Fig. 10), a thin plate 0.25 cm of CPI is bonded on to a rigidized block of insulation (Kaowool or mullite) whose sides are packaged in a thin superalloy foil. This concept is analogous to the RSI concept except that the CPI provides a thicker, more rugged and durable surface, while the foil packaging around the sides simplifies routine inspection to examination of the surface.

These concepts have been tested using scaled-up models in the radiant heat lamp facility in Area 1, Area 2, and Area 2P. Results indicate that more detailed design is required at the attachment points as excessive oxidation of the metallic parts during cycling prevented the freedom of motion of the CPI tile, causing a local buildup of stresses at the support points. This resulted in a slight buckling of the CPI tile.

For the bonded concepts it was found that the rigidized fibrous materials (Kaowool and mullite) did not possess the required thermal shock resistance in themselves to survive the Area 2 and Area 2P re-entry cycling. Failure in the fibrous

insulation occurred at points of maximum thermal stress during re-entry heating. Further work is needed to improve the thermal shock performance of the rigidized fibers.

References

1. Tobin, A., Feldman, C., Russak, M. and Reichman, J., "Development of a Closed Pore Insulation Material," NASA Contract CR-2254, 1972.

2. Varisco, A., Tobin, A., Harris, H. G., "Development and Design Applications of a Closed Pore External Thermal Protection System," NASA Contract NAS 9-12781 (1972).

3. Feldman, C., and Russak, M., "Further Characterization of a Closed Pore Insulating Material," NASA Langley Contract Extension NAS 1-10713 (1973), CR-11295.

4. Geschwind, G., Hershaft, A., Hoff, M. and Jenkins, R., "Environmental Testing of Closed Pore Insulation-I-Arc Jet Testing," Grumman Research Memorandum RM-565 (1973).

5. Feldman, C., and Russak, M., "Environmental Testing of Closed Pore Insulation-II-Salt Spray Testing," Grumman Research Memorandum RM-570 (1973).

6. Wahl, N., "Rain Erosion Characteristics of Thermal Protection System Materials at Subsonic Velocities," AFML-TR-72-145 (1972).

7. Russak, M., "Environmental Testing of Closed Pore Insulation-III-Rain Erosion," Grumman Research Memorandum RM-573.

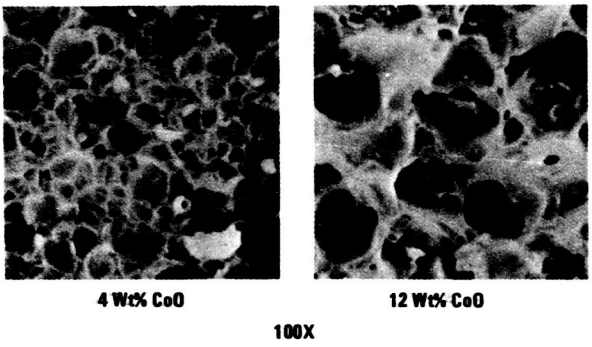

Fig. 1 SEM Photographs of Sintered Cenosphere Bodies Fired at 1650K for 1 Hour

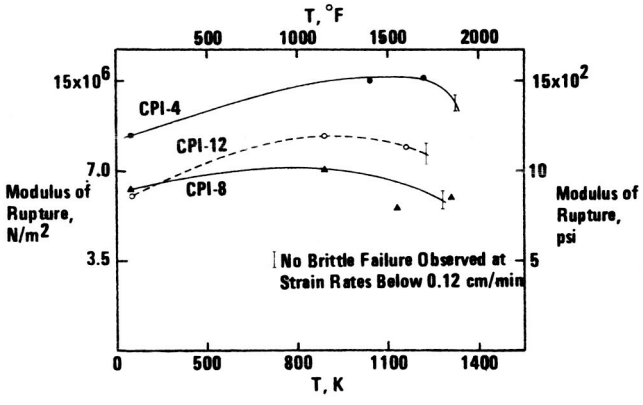

Fig. 2 Elastic Modulus vs Temperature for Three CPI Materials

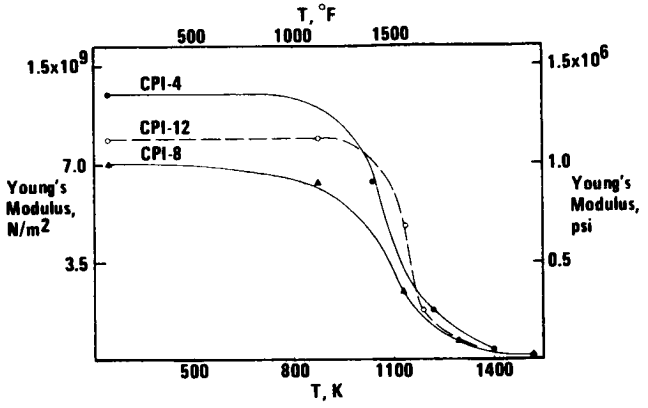

Fig. 3 Modulus of Rupture (Flexure) vs Temperature for Three CPI Compositions

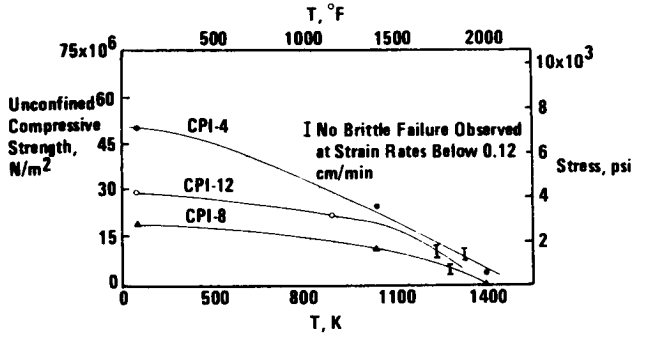

Fig. 4 Compressive Strength vs Temperature for Three CPI Compositions

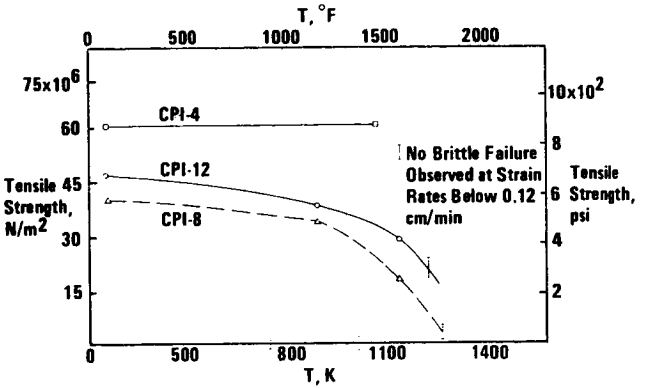

Fig. 5 Tension Strength vs Temperature for Three CPI Compositions

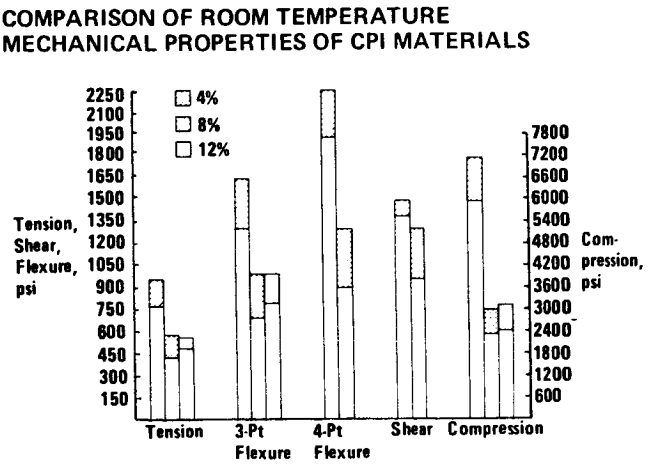

Fig. 6 Comparison of Room Temperature Mechanical Properties of CPI Materials

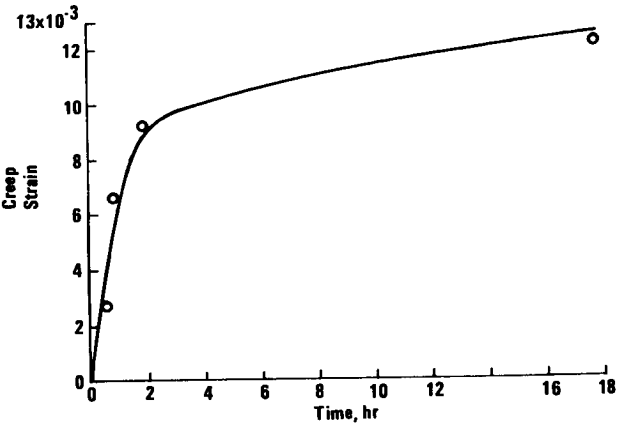

Fig. 7 Flexural Creep Strain vs Time for CPI-8 at 1800°F

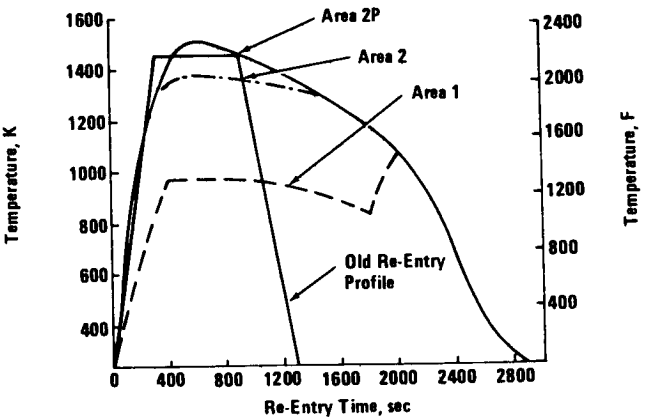

Fig. 8 Modified Re-Entry Thermal Profile

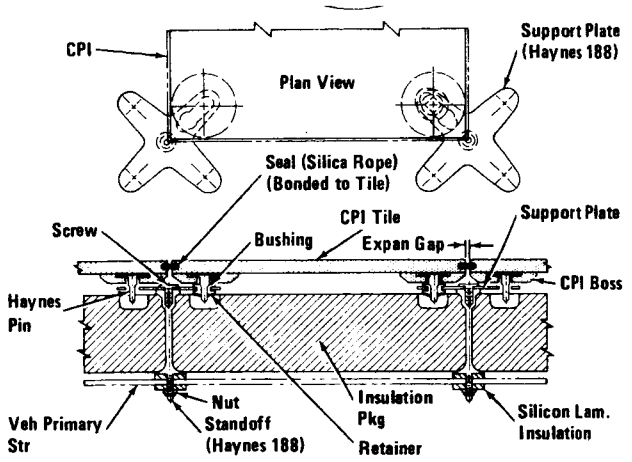

Fig. 9 CPI/Mechanically Supported

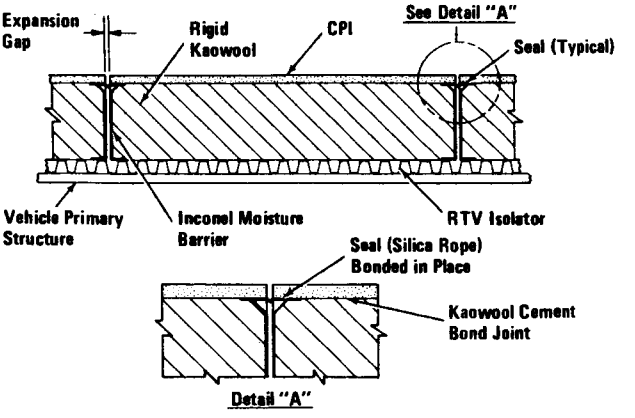

Fig. 10 CPI/Kaowool Bonded Concept